Jour. Ind. Inst. Sc. 61 (A), July 1979, Pp. 105–125

The dielectric-coated conducting sphere—modal and near-field characteristics

PARVEEN WAHID AND R. CHATTERJEE
Department of Electrical Communication Engineering, Indian Institute of Science, Bangalore 560 012

Received on June 27, 1979

Abstract

A modal analysis and near-field study for a dielectric-coated conducting sphere excited by a delta function electric field source has been made. The structure can support an infinite number of modes theoretically. For equatorial excitation only odd order modes are excited, whereas for non-equatorial excitation both even and odd order modes are excited. The variation of the amplitude coefficients both internal and external exhibit a different nature of variation with respect to the various structure parameters for different modes. The field distributions both in the r and θ directions for non-equatorial excitation show good agreement between theory and experiment for the strongest mode.

Key words: Dielectric-coated sphere, dielectric-coated prolate spheroids, modal analysis, excitation.

1. Introduction

Scharfman[1] and Rheinstein[2] have studied the backscatter and total scattering cross-sections of dielectric-coated spheres. Yeh[3] reported studies on dielectric-coated prolate spheroids. Chatterjee *et al* have reported theoretical and experimental work on dielectric-coated conducting spheres excited in the hybrid mode[4] and in the TM symmetric mode[5]. Chatterjee[6] has solved the electromagnetic boundary value problem of the dielectric-coated conducting sphere excited by delta-function electric and magnetic field sources. Chatterjee[7] has also studied the truncated dielectric-coated conducting sphere excited in the TM symmetric mode as an antenna. Chatterjee *et al*[8] have also studied the radiation characteristics of dielectric sphere excited in TM mode.

In the present paper, a modal analysis of the dielectric-coated conducting sphere excited in the symmetric transverse magnetic mode and a study of the near-field characteristics has been made. The theoretical results for the near field have been compared with the experimental results obtained for truncated dielectric-coated conducting spheres.

2. Modal analysis

2.1. *Near-field components*

The geometry of the dielectric-coated conducting sphere is shown in Fig. 1. The dielectric-coated conducting sphere is excited in the symmetric transverse magnetic mode. The source of excitation is assumed to be a delta-function electric field source $E_0 e^{-j\omega t}$ applied normally and uniformly over an annular ring of radius $b \sin \theta_1$ and width $(b - a) \sin \theta_1$.

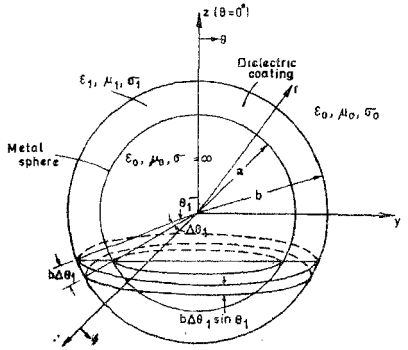

a—inner radius of dielectric-coated conducting sphere

b—outer radius of dielectric-coated conducting sphere

d—$(b - a)$ coating thickness

θ_1—angle of excitation

$\epsilon_0, \mu_0, \sigma_0$—permittivity, permeability and conductivity of free space

$\epsilon_1, \mu_1, \sigma_1$—permittivity, permeability and conductivity of dielectric material

FIG. 1. Geometry of the structure.

Let,

$$E_{r_0} = E_0 \cos \theta_1 \text{ and } E_{\theta_0} = E_0 \sin \theta_1 \tag{1}$$

be the components of E_0 in the r and θ directions respectively, and let

$$E_0 = -\frac{V}{b \triangle\theta \sin \theta_1} \text{ for } \theta_1 - \frac{\triangle\theta_1}{2} < \theta < \theta_1 + \frac{\triangle\theta_1}{2}$$

$$E_0 = 0, \text{ for } \theta < \theta_1 - \frac{\triangle\theta_1}{2} \text{ and } \theta > \theta_1 + \frac{\triangle\theta_1}{2} \tag{2}$$

where V is the excitation voltage applied across the gap $b \triangle\theta_1 \sin \theta_1$ over the annular ring.

The components E_{r_0} and E_{θ_0} can be expanded in a series of spherical harmonics as follows

$$E_{r_0}(r, \theta, \phi) = -\frac{1}{k_1} \sum_{n=1}^{\infty} n(n+1) D_{0n}(r) P_n(\cos \theta) e^{-j\omega t} \tag{3}$$

$$E_{\theta_0}(r, \theta, \phi) = -\frac{1}{k_1} \sum_{n=1}^{\infty} C_{on}(r) P_n'(\cos\theta)\, e^{-j\omega t} \tag{4}$$

where C_{on} and D_{on} are constants assuming that $(b - a) \ll a$ and $\ll b$, *i.e.*, the dielectric-coating is very thin, we have

$$C_{on}(a) \simeq C_{on}(b) = \frac{-k_1(2n+1)}{2\pi n(n+1)} \int_{\phi=0}^{2\pi} \int_{\theta=0}^{\pi} E_0 \sin\theta_1 \cdot \times P_n'(\cos\theta) \sin\theta \, d\theta \, d\phi$$

$$= -\frac{V}{b} k_1 \frac{(2n+1)}{n(n+1)} \sin\theta_1 P_n'(\cos\theta_1) \tag{5}$$

$$D_{on}(a) \simeq D_{on}(b) = \frac{k_1(2n+1)}{2\pi n(n+1)} \int_{\phi=0}^{2\pi} \int_{\theta=0}^{\pi} E_0 \cos\theta_1 \cdot \times P_n(\cos\theta) \sin\theta \, d\theta \, d\phi$$

$$= -\frac{V}{b} k_1 \frac{2n+1}{n(n+1)} \cos\theta_1 P_n'(\cos\theta_1) \tag{6}$$

The field components for the dielectric-coated conducting sphere excited in the symmetric TM mode are given by [6]

Medium I: $a \leqslant r \leqslant b$

$$E_r^i = -\sum_{n=1}^{\infty} n(n+1) P_n(\cos\theta) [L_{on} j_n(k_1 r) + M_{on} y_n(k_1 r)] e^{-j\omega t} + E_{r_0} \tag{7}$$

$$E_\theta^i = -\sum_{n=1}^{\infty} P_n'(\cos\theta) \frac{1}{k_1 r} [L_{on}[k_1 r j_n(k_1 r)]' + M_{on}[k_1 r\, y_n(k_1 r)]'] e^{-j\omega t} + E_{\theta_0} \tag{8}$$

$$H_\phi^i = \sum_{n=1}^{\infty} \frac{k_1}{j\omega\mu_1} P_n'(\cos\theta) [L_{on}\, j_n(k_1 r) + M_{on}\, y_n(k_1 r)] e^{-j\omega t} \tag{9}$$

Medium II: $r \geqslant b$.

$$E_r^e = -\sum_{n=1}^{\infty} n(n+1) P_n(\cos\theta) N_{on} \frac{1}{k_0 r} h_n^{(1)}(k_0 r) e^{-j\omega t} \tag{10}$$

$$E_\theta^e = -\sum_{n=1}^{\infty} P_n'(\cos\theta)\; N_{on}\,\frac{1}{k_0 r}\,[k_0 r\; h_n^{(1)}(k_0 r)]'\; e^{-j\omega t} \tag{11}$$

$$H_\phi^e = \sum_{n=1}^{\infty} \frac{k_0}{j\omega\mu_0}\; P_n'(\cos\theta)\; N_{on}\, h_n^{(1)}(k_0 r)\, e^{-j\omega t} \tag{12}$$

ω is the angular frequency, $P_n'(\cos\theta) = \partial P_n(\cos\theta)/\partial\theta$, $j_n(k_1 r)$, $y_n(k_1 r)$ and $h_n^{(1)}(k_0 r)$ are the spherical Bessel, Neumann and Hankel functions of the first kind respectively. L_{on} and M_{on} are the internal amplitude coefficients and N_{on} are the external amplitude coefficients.

2.2. *Existence of even and odd order modes*

The eqns. (7–12) show that the field inside and outside the dielectric-coated conducting sphere is represented as the sum of an infinite number of modes, even and odd. The existence of odd or even and odd order modes depends on the angle of excitation θ_1, which is involved in the expressions for C_{on} and D_{on} [eqns. (5) and (6)].

When $\theta_1 = 90°$, corresponding to the case of equatorial excitation, eqn. (5) for the coefficient C_{on} becomes

$$C_{on}(a) \simeq C_{on}(b) = -\frac{V}{b}\,\frac{k_1\,(2n+1)}{2n\,(n+1)}\,P_n'(O) \tag{13}$$

where,

$$P_n'(O) = \begin{cases} 0 & \text{for } n \text{ even} \\ \dfrac{j^{n-1}\,2^{1-n}\,n!}{\left[\left(\dfrac{(n-1)}{2}\right)!\right]^2} & \text{for } n \text{ odd.} \end{cases} \tag{14}$$

Therefore taking into account the orthogonality of the modes, [Appendix I] we have the following results.

(i) For equatorial excitation, $\theta_1 = 90°$, only odd order modes exist for the dielectric-coated conducting sphere. Then, the components E_r, E_θ and H_ϕ can be represented as

$$E_r = E_r|_{n=1} + E_r|_{n=3} + E_r|_{n=5} + \cdots \tag{15a}$$

$$E_\theta = E_\theta|_{n=1} + E_\theta|_{n=3} + E_\theta|_{n=5} + \cdots \tag{15b}$$

$$H_\phi = H_\phi|_{n=1} + H_\phi|_{n=3} + H_\phi|_{n=5} + \cdots \tag{15c}$$

(ii) When $\theta_1 \neq 90°$ both even and odd order modes exist on the dielectric-coated conducting sphere. The components can be represented as

$$E_r = E_r|_{n=1} + E_r|_{n=2} + E_r|_{n=3} + \cdots \tag{16a}$$

$$E_\theta = E_\theta|_{n=1} + E_\theta|_{n=2} + E_\theta|_{n=3} + \cdots \tag{16b}$$

$$H_\phi = H_\phi|_{n=1} + H_\phi|_{n=2} + H_\phi|_{n=3} + \cdots \tag{16c}$$

2.3. *Boundary conditions*

The boundary conditions are:

$$\text{(i) } E_\theta^i = E_\theta^s \; ; \; H_\phi^i = H_\phi^s \text{ at } r = b \tag{17}$$

$$\text{(ii) } E_\theta^i = 0 \text{ at } r = a. \tag{18}$$

Using eqns. (7–12) and the boundary conditions, we have

$$\frac{1}{k_1 b}\left[L_{on}\left[k_1 b j_n'(k_1 b)\right]' + M_{on}\left[k_1 \, \mathrm{by}_n'(k_1 b)\right]'\right] + \frac{C_{on}(b)}{k_1} = N_{on}\frac{1}{k_0 b}\left[k_0 b\, h_n^{(1)}(k_0 b)\right]' \tag{19}$$

$$\frac{k_1}{\mu_1}\left[L_{on}\, j_n(k_1 b) + M_{on}\, y_n(k_1 b)\right] = \frac{k_0}{\mu_0} N_{on}\, h_n^{(1)}(k_0 b) \tag{20}$$

$$\frac{1}{k_1 a}\left[L_{on}\left[k_1 a j_n'(k_1 a)\right]' + M_{on}\left[k_1 a y_n'(k_1 a)\right]'\right] + \frac{C_{on}(b)}{k_1} = 0 \tag{21}$$

Using eqn. (5) in the above equations, the amplitude coefficients L_{on}, M_{on} and N_{on} can be uniquely determined for each value of n. The field is thus uniquely determined inside and outside the dielectric-coated conducting sphere for each value of n. Hence it can be concluded that the TM_{on} modes exist for $n = 1,2,3,\cdots$ etc., for this structure.

2.4. *Evaluation of the amplitude coefficients*

The internal and external amplitude coefficients L_{on}, M_{on} and N_{on} have been numerically evaluated for different values of $(b - a)$, a, θ_1, f and ϵ_r. The first six modes have been considered in all the above cases. For the case of equatorial excitation, the odd order modes TM_{01}, TM_{03} and TM_{05} have been considered. All the numerical computations have been carried out with the aid of the IBM 360/44 digital computer.

2.5. *Analysis of the amplitude coefficients*

(i) The variation of the magnitude of the amplitude coefficients with coating thickness is shown in Figs. 2–4. The cases $a = 1{\cdot}0$ to $4{\cdot}0$ cm for constant $\theta_1 = 130°$ have been studied. The variation in the case of equatorial excitation $\theta_1 = 90°$ is shown in Figs. 5–7. The variation is found to be different in each of the cases studied. It is seen that the coefficients M_{on} show only a slight variation with coating thickness.

(ii) The variation of the magnitude of the amplitude coefficients with inner radius a, is shown in Figs. 8–10, for $\theta_1 \neq 90°$ and in Figs. 11–13 for the case of equatorial excitation. The variation has been studied for fixed values of $(b - a) = 0{\cdot}02$, $0{\cdot}08$, $0{\cdot}14$

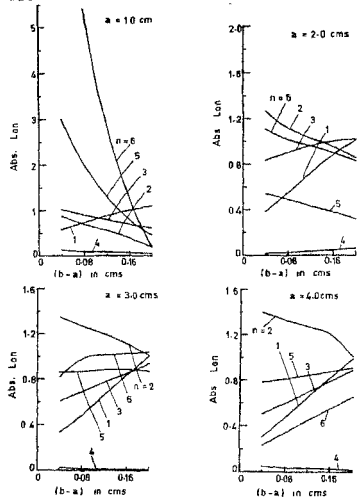

FIG. 2—VARIATION OF INTERNAL AMPLITUDE COEFFICIENTS, Lon, WITH COATING THICKNESS.
f = 9·375 GHz, ε_r = 2·56, θ_1 = 130°

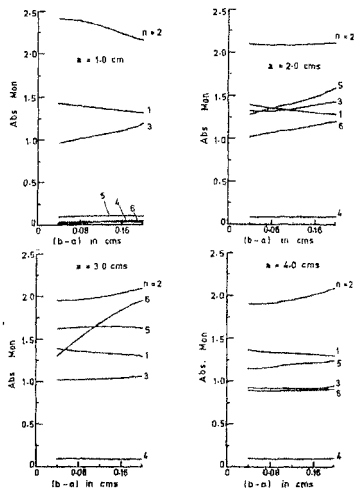

FIG. 3—VARIATION OF THE INTERNAL AMPLITUDE COEFFICIENTS, Mon, WITH COATING THICKNESS
f = 9·375 GHz, ε_r = 2·56, θ_1 = 130°

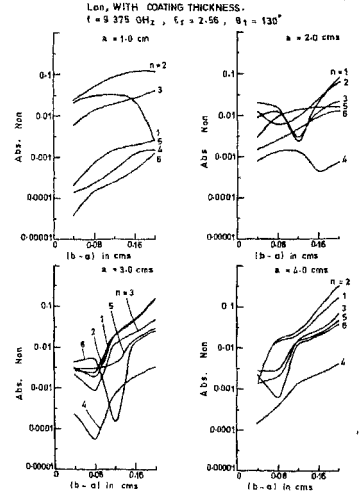

FIG. 4—VARIATION OF THE EXTERNAL AMPLITUDE COEFFICIENTS Mon, WITH COATING THICKNESS
f = 9·375 GHz, ε_r = 2·56, θ_1 = 130°

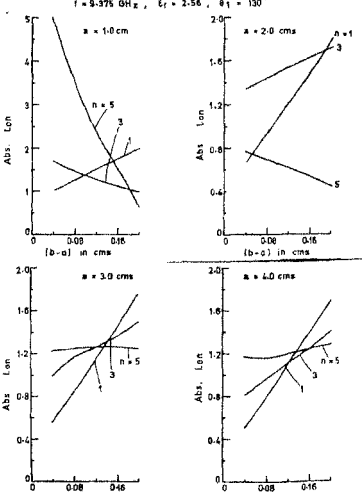

FIG 5—VARIATION OF THE INTERNAL AMPLITUDE COEFFICIENTS, Lon, WITH COATING THICKNESS FOR EQUATORIAL EXCITATION
f = 9·375 GHz, ε_r = 2·56, θ_1 = 90°

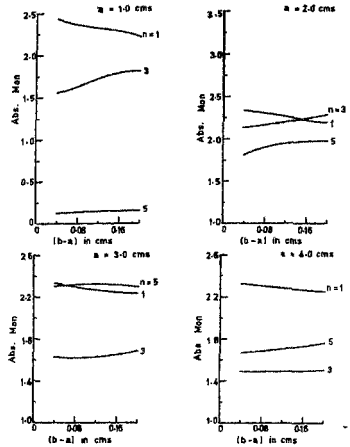

FIG. 6 –VARIATION OF THE INTERNAL AMPLITUDE COEFFICIENTS Mon WITH COATING THICKNESS FOR EQUATORIAL EXCITATION
f = 9·375 GHz , ε_r = 2·56 , θ_i = 90°

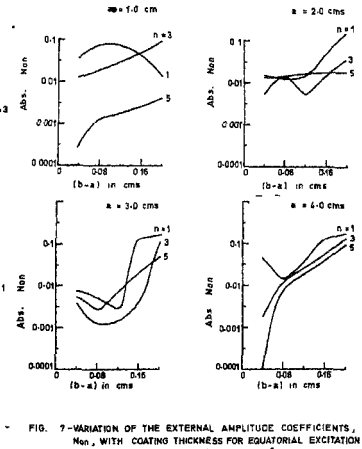

FIG. 7 –VARIATION OF THE EXTERNAL AMPLITUDE COEFFICIENTS, Mon, WITH COATING THICKNESS FOR EQUATORIAL EXCITATION
f = 9·375 GHz , ε_r = 2·56 , θ_i = 90°

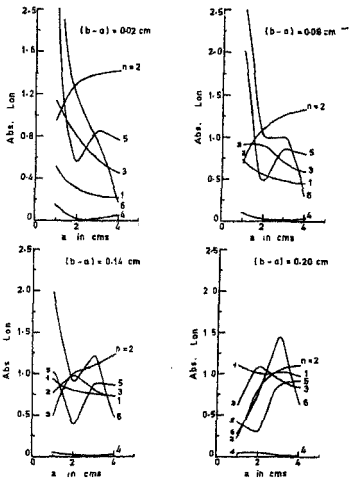

FIG. 8 –VARIATION OF THE INTERNAL AMPLITUDE COEFFICIENTS, Lon , WITH INNER RADIUS 'a'
f = 9·375 GHz , ε_r = 2·56 , θ_i = 130°

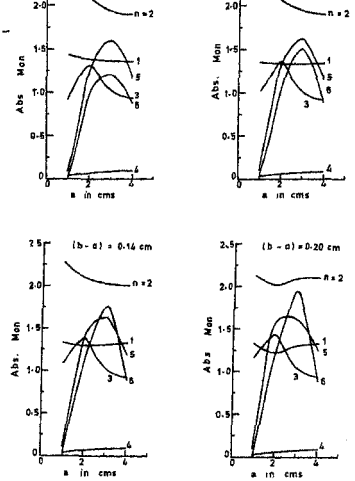

FIG 9 –VARIATION OF THE INTERNAL AMPLITUDE COEFFICIENTS, Mon , WITH INNER RADIUS 'a'
f = 9·375 GHz , ε_r = 2·56 , θ_i = 130°

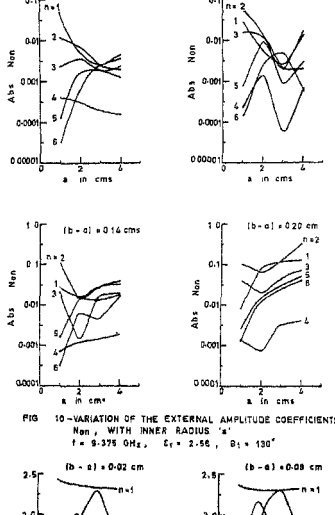

FIG 10 – VARIATION OF THE EXTERNAL AMPLITUDE COEFFICIENTS, Nan , WITH INNER RADIUS 'a'
f = 9·375 GHz , ε_r = 2·56 , θ_1 = 130°

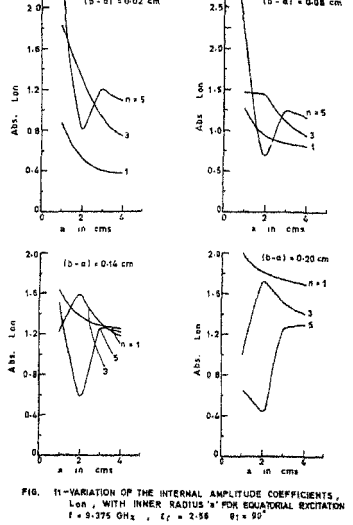

FIG. 11 – VARIATION OF THE INTERNAL AMPLITUDE COEFFICIENTS, Lan , WITH INNER RADIUS 'a' FOR EQUATORIAL EXCITATION
f = 9·375 GHz , ε_r = 2·56 θ_1 = 90°

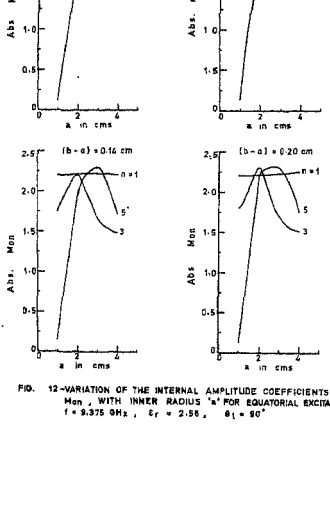

FIG. 12 – VARIATION OF THE INTERNAL AMPLITUDE COEFFICIENTS, Man , WITH INNER RADIUS 'a' FOR EQUATORIAL EXCITATION
f = 9·375 GHz , ε_r = 2·56 , θ_1 = 90°

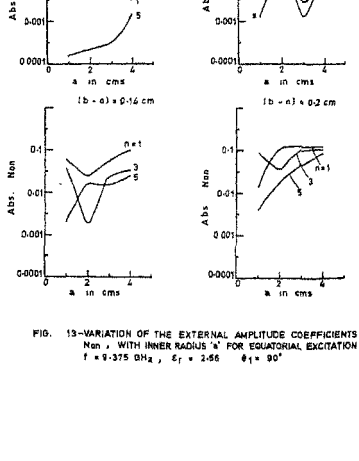

FIG. 13 – VARIATION OF THE EXTERNAL AMPLITUDE COEFFICIENTS, Nan , WITH INNER RADIUS 'a' FOR EQUATORIAL EXCITATION
f = 9·375 GHz , ε_r = 2·56 θ_1 = 90°

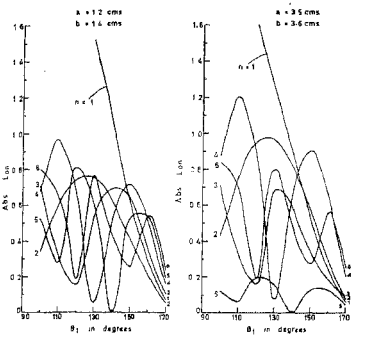

FIG 14—VARIATION OF THE INTERNAL AMPLITUDE COEFFICIENTS, Lon, WITH ANGLE OF EXCITATION θ_1
f = 9·375 GHz, ε_r = 2·56

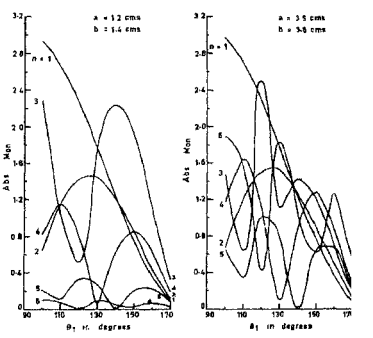

FIG 15—VARIATION OF THE INTERNAL AMPLITUDE COEFFICIENTS, Mon, WITH ANGLE OF EXCITATION θ_1
f = 9·375 GHz, ε_r = 2·56

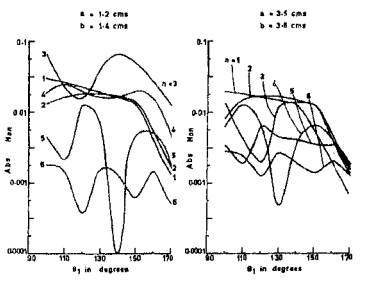

FIG 16—VARIATION OF THE EXTERNAL AMPLITUDE COEFFICIENTS, Mon, WITH ANGLE OF EXCITATION θ_1
f = 9·375 GHz, ε_r = 2·56

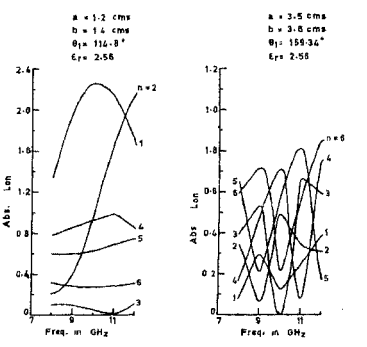

FIG 17—VARIATION OF THE INTERNAL AMPLITUDE COEFFICIENTS, Lon, WITH FREQUENCY OF EXCITATION

and 0·2 cm for fixed values of a ranging from 1·0 to 4·0 cm. The variation is found to be different for each individual mode.

(iii) The variation of the magnitude of L_{0n}, M_{0n} and N_{0n} with angle θ_1 for θ_1 ranging from 100° to 160° keeping the other parameters fixed is shown in Figs. 14 to 16. The variation for all the three coefficients is found to be oscillatory going through various maximum and minimum values for each of the individual modes for different values of θ_1

(iv) A study of the variation of the amplitude coefficients with the frequency of excitation for fixed values of a, b and θ_1 has been made in the range 8·0 to 12·0 GHz. The results for the case $\theta_1 \neq 90°$ and $\theta_1 = 90°$ are shown in Figs. 17–19 and Fig. 20 respectively.

(v) The variation of the magnitude of the amplitude coefficients with the relative permittivity of the coating material is shown in Fig. 21 for the case $\theta_1 \neq 90°$ and in Fig. 22 for the case $\theta = 90°$. The values of ϵ_r ranging from 2·08 to 700·0 corresponding to the various dielectric materials given in Appendix II have been considered. The magnitude of the amplitude coefficients is found to be sensitive to the value of ϵ_r. All the coefficients L_{0n}, M_{0n} and N_{0n} have a maximum and a minimum value for a particular value of ϵ_r.

The above considerations regarding the behaviour of the amplitude coefficients of the dielectric-coated conducting sphere can be explained on the basis of the functional dependance of the amplitude coefficients which involve the spherical Bessel, Neumann and Hankel functions (eqns. 19-21).

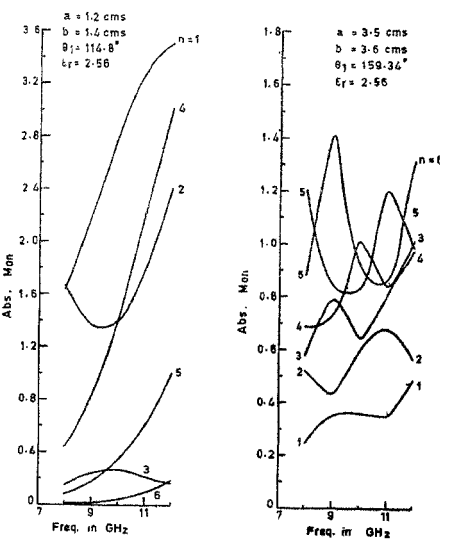

FIG. 18. Variation of the internal amplitude coefficients, M_{0n} with frequency of excitation.

3. Near-field characteristics

The expressions for the field components outside the dielectric-coated conducting sphere are given in eqns. (10–12). The external amplitude coefficients N_{0n} are determined from eqns. (19–21).

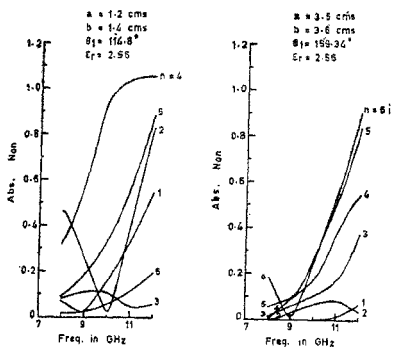

FIG. 19. Variation of the external amplitude coefficients, N_{on}, with frequency of excitation.

The variation of the field components with θ and the radial field decay of these components has been studied theoretically for the first six modes for different dielectric-coated conducting spheres at the frequency of excitation $f = 9{\cdot}375$ GHz. Figure 23 shows the variation with θ of the power normalized with respect to the maximum value for individual modes and Fig. 24 shows the radial field decay of the components for the individual modes.

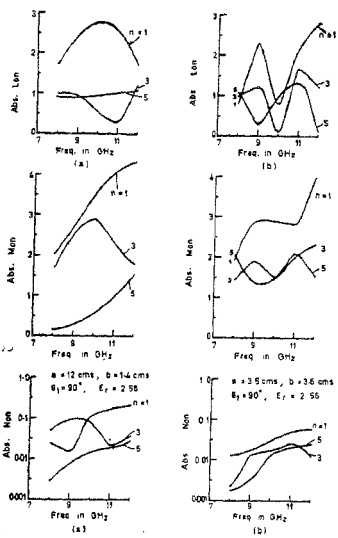

FIG. 20. Variation of the amplitude coefficien L_{on}, M_{on} and N_{on} with frequency of excitatio for equatorial excitation.

4. Experimental measurement of the near-field characteristics

4·1. *Truncated dielectric-coated conducting spheres*

In order to verify the theoretical investigations, truncated dielectric-coated conducting spheres of different dimensions were made. The conducting sphere was made of brass and it was coated with perspex. The truncated dielectric-coated conducting sphere is terminated in a dielectric-coated cylindrical portion which tapers to a point as a dielectric-coated conducting cone to achieve impedence matching at the feed end (Fig. 25 (i)).

To excite the symmetric TM mode on the truncated dielectric-coated conducting sphere a mode transducer is used. The mode transformation is as follows:

(i) Rectangular waveguide (TE_{10} mode) to

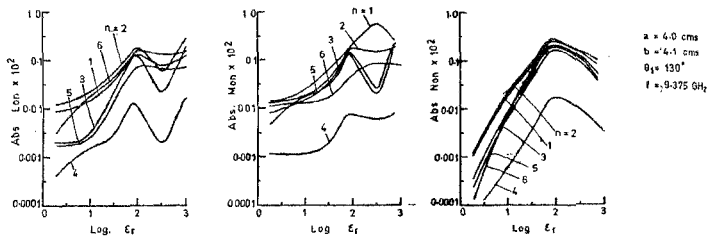

FIG. 21. Variation of the amplitude coefficients with ϵ_r the relative permittivity of the coating material.

(ii) Coaxial line (TEM mode) to

(iii) Truncated dielectric-coated conducting sphere (TM_{0n} mode).

A sketch of the truncated dielectric-coated conducting sphere with the arrangement for excitation from a rectangular to coaxial transducer is shown in Fig. 25 (ii). The specifications of the structures used are given in Appendix III.

4.1.1. *Experimental investigations*

(*a*) *Radial field decay* : The arrangement used for measuring the radial field decay is shown in Fig. 26 *a*. The field components E_r, E_θ and H_ϕ are measured using the appropriate probes. The probe is placed very close to the surface of the structure along an axis corresponding to $\theta = 30°$, so that the even and odd order modes that exist on the structure are taken into account. A view of the structure and the probe is shown in Fig. 26 *b*. The experimental results are given in Figs. 27–29 along with the theoretical results for comparison.

(*b*) *Variation of the field components with* θ : The arrangement for the measurement of the variation of the components E_r, E_θ and H_ϕ with the angle θ is shown in

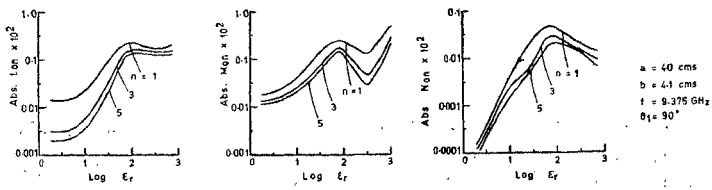

FIG. 22. Variation of the amplitude coefficients with ϵ_r the relative permittivity of the coating material for equatorial excitation.

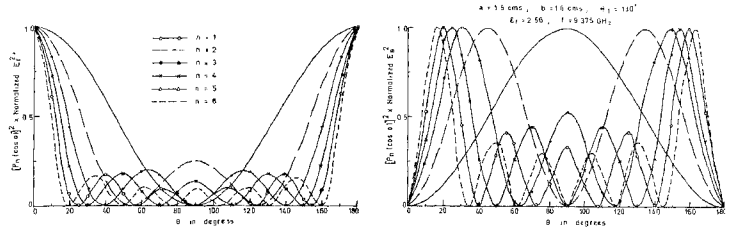

FIG. 23. Variation of normalized power with θ for the first six modes.

Fig. 26 *c*. The probe is placed close to the surface of the structure. The experimental results are given in Figs. 30–32. The theoretical results are also shown for comparison.

5. Analysis

(i) *Radial decay* : The agreement between the theoretical curve for the strongest mode and the experimental curve is good for the components E_r, E_θ and H_ϕ (Figs. 27–29). The mode for which the external amplitude coefficient N_{sn} is found to have the maximum value has been termed the strongest mode of the dielectric-coated conducting sphere.

(ii) *Variation with* θ : It is seen that there is good agreement between the experimental results and the theoretical results obtained for the strongest mode for the components E_r, E_θ and H_ϕ in all cases (Figs. 30–32).

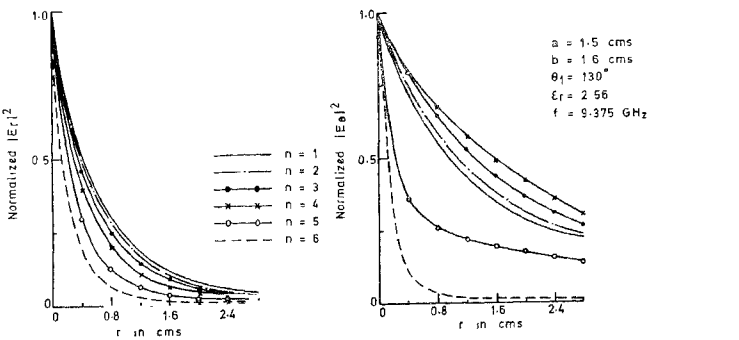

FIG. 24. Radial field decay for the first six modes.

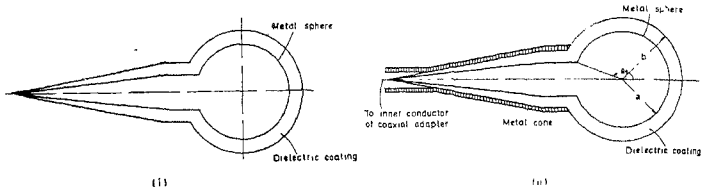

FIG. 25. (i) Sketch of the truncated dielectric-coated conducting sphere.
(ii) Sketch of the method of excitation.

An attempt has been made to make a comparative study of the experimental curve and the theoretical curve obtained by the summation of the first six modes (since the modes are orthogonal) for the near field (Figs. 33, 34).

(i) *Radial field decay* : As the components H_ϕ and E_θ have a similar functional variation, only the E_r and E_θ components have been considered. The radial decay

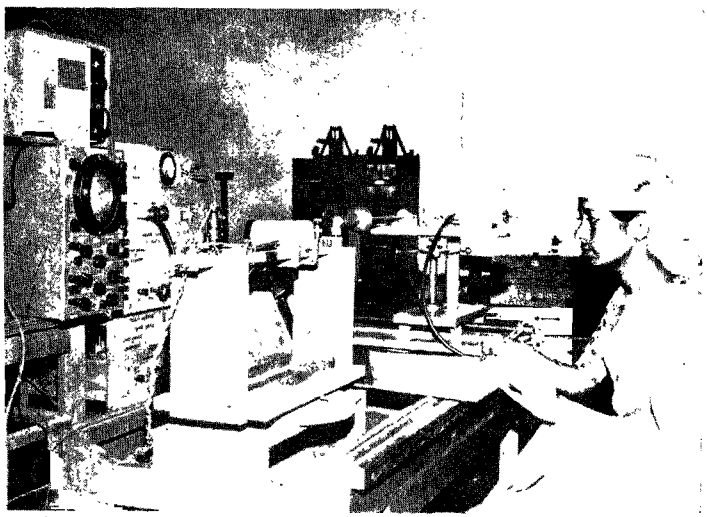

FIG. 26 (*a*). Experimental set-up for the measurement of the near field decay.

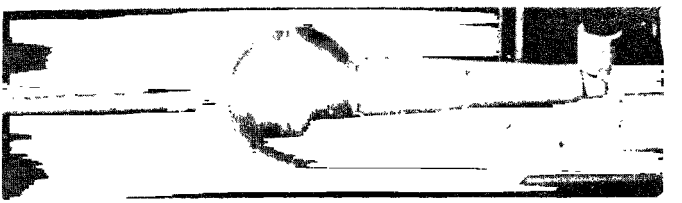

FIG. 26 (*b*). A view of the field sampling probe and the truncated dielectric-coated conducting sphere.

for the E_r component shows fair agreement with experiment not only for the strongest mode but also when compared with the combined modes whereas for the E_θ component the radial decay for the combined modes exhibits an oscillatory nature (Fig. 33). This may probably be explained on the basis of the nature of the functions involved, *i.e.*

$$E_\theta = \sum_n \text{const.}\ I'_n(\cos\theta)\frac{1}{k_{0r}}\left[k_{or}\, i_n^{(1)}(k_{0r})\right]'.$$

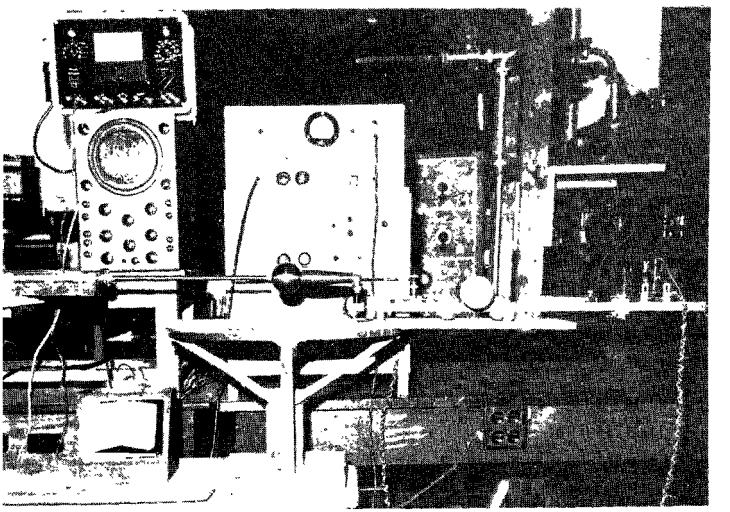

FIG. 26 (*c*). Experimental set-up for the measurement of the near field variation with θ.

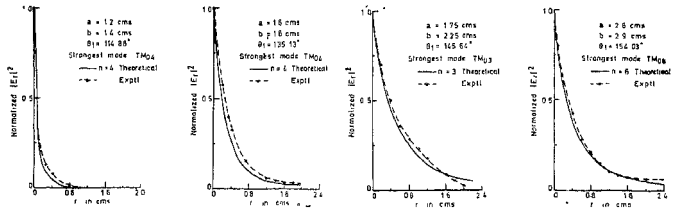

FIG. 27 (*a*). Radial field decay of normalized $|E_r|^2$. $f = 9{\cdot}375$ GHz, $\epsilon_r = 2{\cdot}56$.

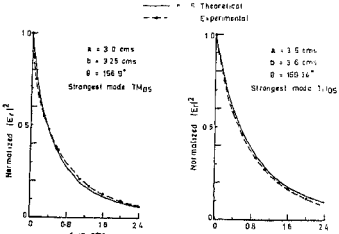

FIG. 27 (*b*). Radial field decay of normalized $|E_r|^2$. $f = 9{\cdot}375$ GHz, $\epsilon_r = 2{\cdot}56$.

(ii) *Variation with* θ : The variation of the near-field components with θ has been measured by placing the appropriate probe very close to the surface of the dielectric-coated conducting sphere. The experimental curve, the theoretical curve for the strongest mode only and for the combined modes for the E_r and E_θ components are given in Fig. 34. It is seen that there is good agreement between the experimental curve and the theoretical curve for the strongest mode.

The comparative study of the theoretical and experimental results shows that the agreement is better in the case of the larger dielectric-coated conducting spheres than in the case of the smaller dielectric-coated conducting spheres (Figs. 27–29). Since the coating thickness has been assumed to be small, by large dielectric-coated conducting spheres it is meant large values of a. Since the mode transducer used is the same, it is obvious that in the case of the smaller dielectric-coated conducting spheres the probe is closer to the discontinuity present at the junction between the dielectric-coated con-

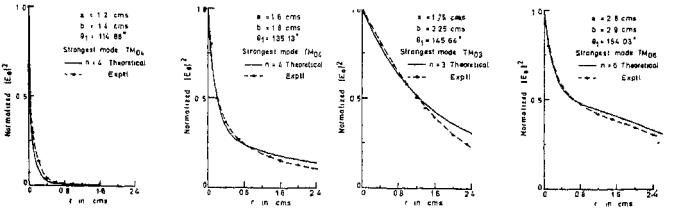

FIG. 28 (*a*). Radial field decay of normalized $|E_\theta|^2$. $f = 9{\cdot}375$ GHz, $\epsilon_r = 2{\cdot}56$.

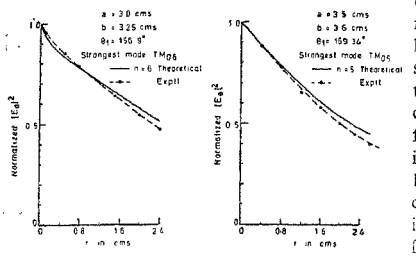

FIG. 28 (*b*). Radial field decay of normalized $|E_\theta|^2$. $f = 9{\cdot}375$ GHz, $\epsilon_r = 2{\cdot}56$.

ducting sphere and the mouth of the mode transducer, compared to the larger dielectric-coated conducting sphere. Hence it is possible that the direct radiation due to the discontinuity interferes with the near field of the dielectric-coated conducting sphere sampled by the probe. In the case of the larger dielectric-coated sphere, however, the probe is at a comparatively larger distance from the junction and the effect of the discontinuity field may not be appreciable. It may therefore be said that the field samples mostly the near field of the dielectric-coated conducting sphere in the case of the larger dielectric-coated conducting spheres without being influenced much by the interfering field.

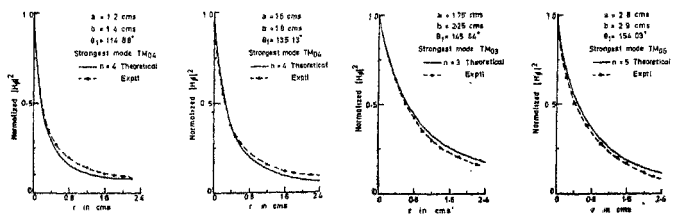

FIG. 29. Radial field decay of normalized $|H_\phi|^2$ $f = 9{\cdot}375$ GHz, $\epsilon_r = 2{\cdot}56$.

Since the rate of decay of the field in the r direction in the case of the smaller dielectric-coated conducting spheres is very fast, the probe output becomes very small when it is placed away from the surface of the dielectric-coated conducting sphere. Hence no further study of the interfering field in the case of the smaller dielectric-coated conducting sphere could be made with the available equipment.

6. Conclusions

The following conclusions can be drawn from the above investigations:

(i) The dielectric-coated conducting sphere can be excited in an infinite number of symmetric TM modes by a delta-function electric field source.

(ii) The existence of even and odd order or odd order modes only is determined by the angle of excitation θ_1.

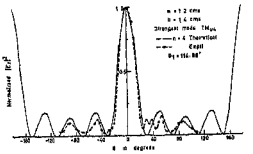

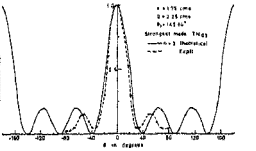

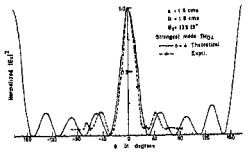

FIG 30a—VARIATION OF NORMALIZED $|E_\theta|^2$ WITH θ
f = 9.375 GHz, ε_r = 2.56

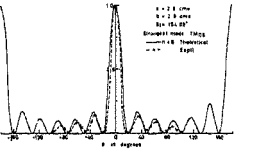

FIG 30b—VARIATION OF NORMALIZED $|E_\theta|^2$ WITH θ
f = 9.375 GHz, ε_r = 2.56

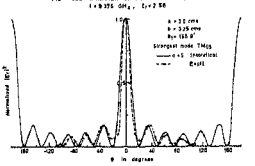

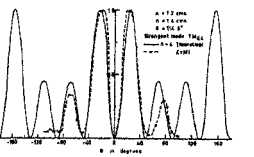

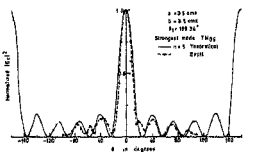

FIG 30c—VARIATION OF NORMALIZED $|E_\theta|^2$ WITH θ
f = 9.375 GHz, ε_r = 2.56

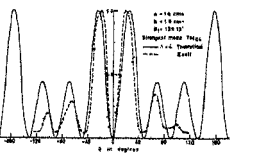

FIG 31a—VARIATION OF NORMALIZED $|E_\theta|^2$ WITH θ
f = 9.375 GHz, ε_r = 2.56

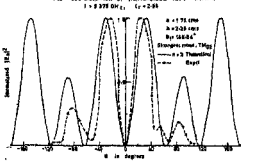

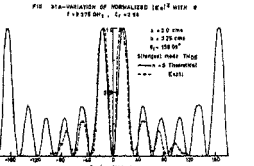

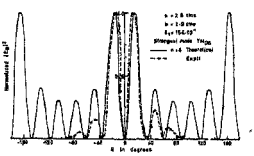

FIG 31b—VARIATION OF NORMALIZED $|E_\theta|^2$ WITH θ
f = 9.375 GHz, ε_r = 2.56

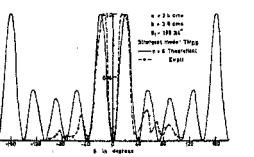

FIG 31c—VARIATION OF NORMALIZED $|E_\theta|^2$ WITH θ
f = 9.375 GHz, ε_r = 2.56

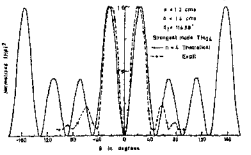

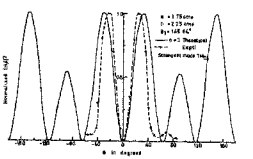

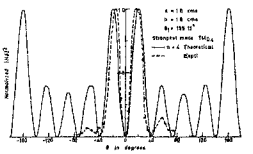

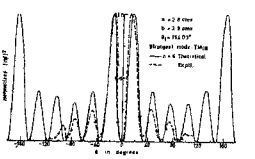

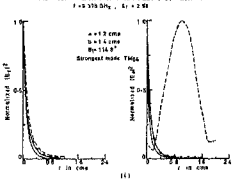

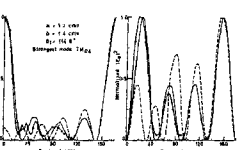

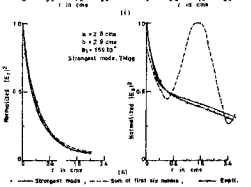

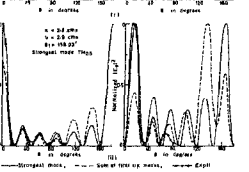

(iii) The internal and external amplitude coefficients are sensitive to the various structure parameters to varying extents.

(iv) The truncated dielectric-coated conducting sphere excited by a coaxial line has very nearly the same field configuration as one of the TM_{on} modes.

(v) The theoretical field distributions obtained in the case of a complete dielectric-coated conducting sphere and the measured near field curves at a frequency of 9·375 GHz agree fairly well.

7. Acknowledgements

The authors are grateful to Dr. S. Dhawan, Director, Indian Institute of Science, for giving all the facilities for the work and to the Council of Scientific and Industrial Research for the sanction of a scheme on this subject.

References

1. SCHAFFMAN, H. — Scattering from dielectric-coated spheres in the region of first resonance, *Jour. Appl. Phy.*, 1954, **25**, 1352.

2. RHEINSTEIN, J. — Scattering of electromagnetic waves from dielectric-coated conducting spheres, *IEEE Trans.*, 1964, *AP*-**12**, 334.

3. YEH, C. W. H. — On the dielectric-coated prolate spheroidal antenna, *Jour. Math. Phys.*, 1963, **42**, 68.

4. CHATTERJEE, R., KESHAVAMURTHY, T. L. AND VEDAVATHY, T. S. — Dielectric-coated spherical metal antennas excited in the unsymmetric hybrid mode at microwave frequencies, *Jour. Inst. Electronic. Telecom. Engs. India*, 1974, **20** (8), 386.

5. CHATTERJEE, R., VEDAVATHY, T. S., PARVEEN WAHID AND NAGESH, B. K. — Dielectric-coated metal spherical antennas excited in the symmetrical TM mode at microwave frequencies, *I.E.E.-I.E.R.E. Proceedings, India*, 1974, **12** (3), 888.

6. CHATTERJEE, R. — Electromagnetic boundary value problem of the dielectric-coated conducting sphere excited by delta-function electric and magnetic sources. *Jour. Ind. Inst. Sc.*, 1974, **56** (3), 167.

7. CHATTERJEE, R. AND PARVEEN WAHID — Truncated dielectric-coated conducting sphere excited in the TM-symmetric mode as an antenna, *I.E.E.-I.E.R.E. Proceedings, India*, 1977, **15** (5), 195.

8. CHATTERJEE, R. AND BHATTACHARYA, A. K. — Modal and radiation characteristics of the dielectric sphere excited in TM symmetric mode, *Jour. Ind. Inst. Sc.*, 1977, **59** (A), 419.

Appendix I

Orthogonality of the modes

The condition for mode orthogonality may be stated mathematically as

$$\int_{\tau} f(r, \theta, \phi)\ \ g(r, \theta, \phi)\, d\tau = 0.$$

where f and g represent the functional variation of two modes.

For the dielectric-coated conducting sphere, considering any two modes, TM_{on} and $TM_{on'}$, where $n \neq n'$, we have for the magnetic field component H_{ϕ}^{i},

$$I = 2\pi \left[\frac{k_1}{i\omega\mu_1}\right]^2 \int_{r=a}^{b} [L_{on}\, j_n(k_1 r) + M_{on}\, y_n(k_1 r)]$$

$$[L_{on'} j_{n'}(k_1 r) + M_{on'} y_{n'}(k_1 r)]\, r^2\, dr \int_{\theta=0}^{\pi} P_n'(\cos\ \theta).$$

$$\times P_{n'}'(\cos\ \theta)\ \sin\ \theta\ \ d\theta.$$

Using the property of Legendre polynomials that

$$\int_{-1}^{+1} P_n(x)\ P_m(x)\ dx = 0 \text{ for } n \neq m, \text{ we have } I = 0.$$

Hence the $TM_{\phi n}$ and $TM_{\phi n'}$ modes are orthogonal. The orthogonality can be proved similarly in the case of the E_r and E_θ components.

Appendix II

Dielectric material considered for the theoretical study

Dielectric material	Relative permittivity	Loss tangent
Teflon	2·08	0·00037
Mycalex 400	7·12	0·0033
Ceramic	28·9	0·0020
Titanium dioxide	85·8	0·0020
Strontium titanate	312·5	0·0006
Barium titanate	700·0	0·0005

Appendix III

Specifications of the truncated dielectric coated conducting spheres

Inner radius a cm	Outer radius b cm	Angle of excitation θ_1 degrees
1·2	1·4	114·8
1·6	1·8	135·1
1·75	2·25	145·6
2·8	2·9	154·0
3·0	3·25	156·9
3·5	3·6	159·3